Implementation of vibrational phase contrast coherent anti-Stokes Raman scattering microscopy

Martin Jurna, Jennifer L. Herek, and Herman L. Offerhaus*

Optical Sciences group, MESA+ Institute for Nanotechnology, Faculty of Science and Technology (TNW),
University of Twente, the Netherlands

*Corresponding author: h.l.offerhaus@utwente.nl

Detection of molecules using vibrational resonances in the fingerprint region for narrowband coherent anti-Stokes Raman scattering (CARS) is challenging. The spectrum is highly congested resulting in a large background and a reduced specificity. Recently we introduced vibrational phase contrast CARS (VPC-CARS) microscopy as a technique capable of detecting both the amplitude and phase of the CARS signal, providing background-free images and high specificity. In this paper we present a new implementation of VPC-CARS based on a third-order cascaded phase-preserving chain, where the CARS signal is generated at a single (constant) wavelength independent of the vibrational frequency that is addressed. This implementation will simplify the detection side considerably.   © 2011 Optical Society of America

OCIS codes: 190.4410, 300.6230, 300.6310.

1. Introduction

CARS microscopy is a noninvasive and label-free imaging technique. Narrowband CARS allows selective excitation of specific of molecular vibrations and can produce high resolution images within seconds [1]. Matching the difference frequency of the pump and Stokes input wavelengths to a vibrational mode of a molecule resonantly enhances the probed CARS (anti-Stokes) output signal. A major drawback is that there is also a CARS signal that is created without this resonant interaction. In the more congested vibrational areas around $800–1600\,\mathrm{cm^{-1}}$, the total signal contains contributions from many closely spaced resonances and the vibrationally insensitive electronic nonresonant signal. The real and imaginary parts of all the vibrations mix together with the real nonresonant response and the total signal becomes too complex to unravel when only detecting the intensity of the CARS signal.

Depending on the ratio of resonant to nonresonant signal, the nonresonant signal can overwhelm the small resonant signal. Samples that contain mixtures of compounds, such as proteins in cells, give rise to a significant nonresonant signal, observed as a background over the full image. The intensity differences in such images are not based on chemical selectivity alone, but contain interferences between the resonant and nonresonant signals. In recent years, various solutions have been developed to overcome the nonresonant background problem based on amplitude [2,3], phase [4,5,7], time [8], or polarization [9,10].
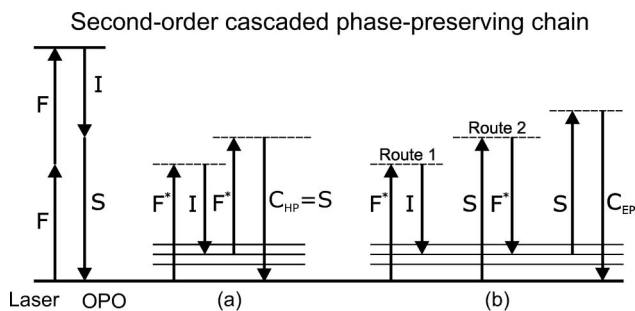
Recently we introduced VPC-CARS microscopy [11], which can remove the nonresonant background signal by detection of the amplitude and phase of the oscillators in the detection volume. The phase is measured with respect to the local excitation fields using a cascaded second-order phase-preserving chain. The cascaded chain starts with a picosecond laser. The second harmonic of this laser pumps an optical parametric oscillator (OPO). CARS is generated using the idler from the OPO and the fundamental of the pump laser. The signal from the OPO serves as the local oscillator. The OPO is tuned to address different vibrational frequencies. As the OPO scans, the CARS output wavelength also scans. Because the singly resonant OPO cannot operate close to degeneracy, the

frequency range that can be addressed is limited from 900–3200 cm^{-1}. In this chain the phases of the CARS signal and local oscillator signal are locked and preserved while selecting different vibrational resonances [12].

Here we expand the VPC-CARS microscopy scheme to a *third*-order cascaded phase-preserving chain. The proposed new detection scheme offers background-free imaging capabilities over the full vibrational spectrum, as well as a significantly simpler implementation. Only a single set of filters and detectors is required to access the entire vibrational spectrum. In this article we discuss the detection scheme, requirements, and advantages.

2. Second- and Third-order Cascaded Phase-preserving Chains

The second-order cascaded phase-preserving chain is shown in Fig. 1(a). The table shows the wavelength and phase relations in the different stages of the chain. The excitation phase is obtained using the interference between two routes addressing a vibrational resonance or virtual state, see Fig. 1(b). In 1997, Chen [13] presented a CARS approach for measuring the vibrational spectrum of a molecule while detecting at a single (constant) wavelength. The third harmonic (355 nm) of an Nd:YAG laser (1064 nm) was used to synchronously pump an OPO. CARS spectra were obtained using the OPO idler as the pump wavelength, the fundamental of the laser as the Stokes wavelength, and the OPO signal as the probe wavelength. The generated CARS signal has a wavelength of 532 nm, corresponding to the second harmonic of the Nd:YAG laser, and maintains this wavelength over the full scanning range. Hence, a complete spectrum can be measured simply by

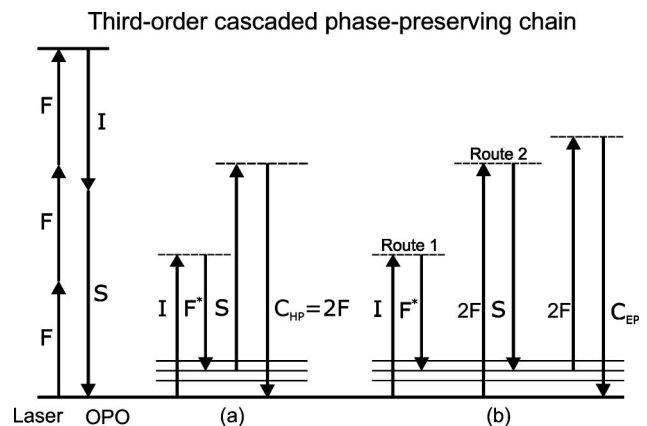tuning the OPO and detecting only at a single wavelength.

The combination of single wavelength detection and the VPC-CARS scheme provides the basis for the third-order phase-preserving chain. Figure 2 shows schematically how the signal and idler from an OPO are created by the third harmonic of a laser. Heterodyne CARS (H-CARS) is obtained with the OPO idler as the pump wavelength, the laser fundamental as the Stokes wavelength, and the OPO signal as the probe wavelength. The CARS signal is now produced at a single wavelength, independent of the tuning of the OPO. Furthermore, it has the same wavelength as the second harmonic of the laser, see Fig. 2(a). The table shows the wavelengths and phase relations of the third-order chain. The wavelengths and phases of the generated CARS signal and second harmonic of the laser are locked, allowing them to interfere with each other.

Detection of the excitation phase is achieved by the combination of route one (OPO idler minus fundamental) and route two (second harmonic of the laser minus OPO signal). In this case, the CARS signal is generated by probing the interference with the second harmonic of the laser, see Fig. 2(b).

3. Differences in Detection

A. Modulation Frequency

In the second-order chain the fundamental wavelength is frequency modulated to allow detection of the interference between the generated CARS signal

Fig. 1. Schematic of the second-order cascaded phase-preserving chain showing the laser, OPO, and CARS process, where (a) shows the heterodyne phase detection scheme and (b) shows the local excitation phase detection scheme. F, fundamental laser; F*, modulated fundamental laser; I, OPO idler; S, OPO signal; C, CARS signal; HP, heterodyne phase; and EP, excitation phase. The table shows the wavelength and phase relations within the heterodyne detection scheme.

Process	Wavelength relation	Phase relation
1. SHG	$2 \cdot \omega_F = \omega_{2F}$	$2 \cdot \phi_F = \phi_{2F}$
2. OPO	$\omega_{2F} = \omega_S + \omega_I$	$\phi_{2F} = \phi_S + \phi_I$
3. CARS	$\omega_{CARS} = 2 \cdot \omega_F - \omega_I$	$\phi_{CARS} = 2 \cdot \phi_F - \phi_I + \phi_{\chi^3}$
4. PPC	$\omega_{CARS} = \omega_S$	$\phi_{CARS} = \phi_S + \phi_{\chi^3}$

Fig. 2. Schematic of the third-order cascaded phase-preserving chain showing the laser, OPO, and CARS process, where (a) shows the heterodyne phase detection scheme and (b) shows the local excitation phase detection scheme. F, fundamental laser; F*, modulated fundamental laser; 2F, second harmonic of the laser; I, OPO idler; S, OPO signal; C, CARS signal; HP, heterodyne phase; and EP, excitation phase. The table shows the wavelength and phase relations within the heterodyne detection scheme.

Process	Wavelength relation	Phase relation
1. SHG	$2 \cdot \omega_F = \omega_{2F}$	$2 \cdot \phi_F = \phi_{2F}$
2. THG	$3 \cdot \omega_F = \omega_{3F}$	$3 \cdot \phi_F = \phi_{3F}$
3. OPO	$\omega_{3F} = \omega_S + \omega_I$	$\phi_{3F} = \phi_S + \phi_I$
4. CARS	$\omega_{CARS} = \omega_I - \omega_F + \omega_S$	$\phi_{CARS} = \phi_I - \phi_F + \phi_S + \phi_{\chi^3}$
5. PPC	$\omega_{CARS} = \omega_{2F}$	$\phi_{CARS} = \phi_{2F} + \phi_{\chi^3}$

and the OPO signal. The beat frequency between the CARS signal and the OPO signal is doubled with respect to the modulation frequency because the fundamental contributes twice in the CARS generation process. In the excitation phase, detection of the fundamental is forward shifted in route one and backward shifted in route two, resulting in twice the modulation frequency as the detected beat frequency.

In the third-order chain the fundamental or second harmonic must be modulated, but now the interference appears at the beat frequency for the detection of the CARS and the detection of the excitation phase. In both cases, the frequency modulator should provide pure frequency modulation without amplitude modulation.

B. Wavelength Detection

The second- and third-order chains produce CARS signals in different wavelength regions. In Fig. 3, graphs are shown for the two different scenarios. The second-order chain is based on an OPO pumped by the second harmonic of an Nd:YAG laser

(1064 nm) (Fig. 3(a)). The third-order chain is based on an OPO pumped by the third harmonic of a laser operating at 1500 nm (Fig. 3(b)). In both scenarios, a lithium triborate-based OPO, pumped around 500 nm is selected, because these are commercially available. The 1064 nm laser is also commercially available. However, a 1500 nm picosecond laser with sufficient power in the third harmonic is not yet available. The third harmonic (355 nm) of a 1064 nm laser is not considered, due to the anticipated additional problems, such as increased two-photon absorption, cell damage, and two-photon enhanced nonresonant background [14,15].

From Fig. 3 it can be seen that the H-CARS signal in the third-order chain has a constant wavelength and the local excitation phase CARS (EP-CARS) signal is always lower in wavelength. In particular

$$\lambda_{\text{F}} > \lambda_{\text{OPO}_{\text{idler}}} > \lambda_{\text{OPO}_{\text{signal}}} > \lambda_{\text{H-CARS}} > \lambda_{\text{EP-CARS}}. \quad (1)$$

This results in a single optimized filter set in combination with a matching detector for the detection of the H-CARS and EP-CARS signal, which is not possible for the second-order chain, where multiple filter sets are needed to cover the full vibrational spectrum.

Furthermore, the cavity mirror set of the OPO determines how close it can be tuned toward the degeneracy point. In the case of the second-order chain, being unable to tune close toward the degeneracy point excludes the lower frequency vibrational resonances (fingerprint region) from the covered vibrational range. The third-order chain can go all the way to the low frequencies as these are reached away from degeneracy. The chain does not reach the highest frequency vibrational resonances. CARS microscopy has proven its use in the high frequency range and does not seem to require the phase detection there as badly because the spectra are less congested. This range can be reached (without phase detection and with a scanning CARS wavelength) if the signal and idler are used for the generation of CARS. In the future, the lower frequency range is expected to become more important to improve chemical selectivity.

4. Conclusion and Discussion

When a laser source becomes commercially available for effective pumping of the OPO with the third harmonic of the laser (around 500 nm), the third-order cascaded phase-preserving chain can be used for sensitive detection of vibrational resonances. This method based on the VPC-CARS scheme and single wavelength detection could attract more commercial interest, due to its background-free imaging capabilities over the full vibrational spectrum and its simplicity for the user. The filters and detectors do not need to be changed and can be designed specifically for this application. Compared to stimulated Raman scattering (SRS) [16], which is inherently free from the electronic nonresonant contribution, this
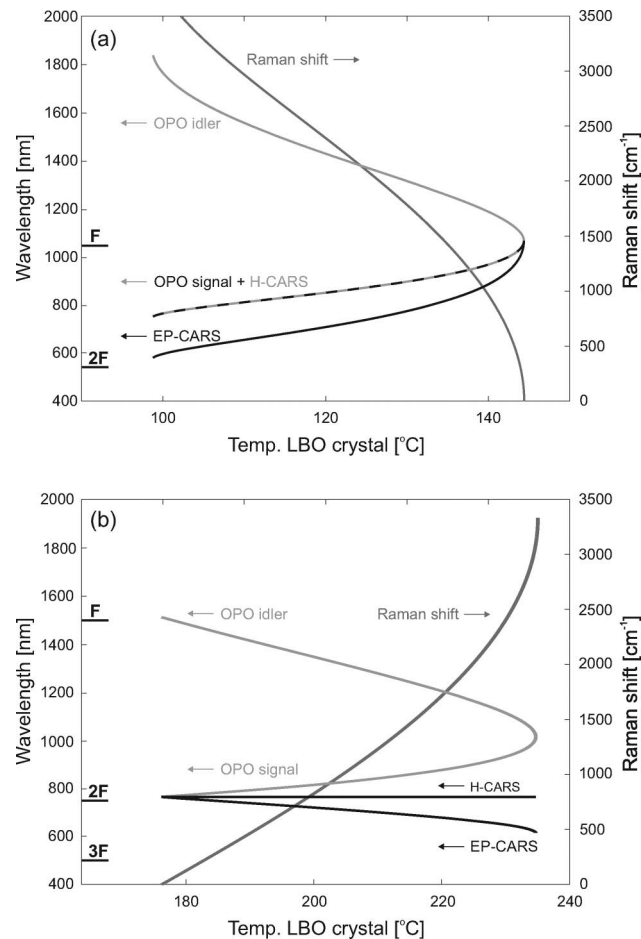
Fig. 3. OPO tuning curves. The OPO signal and idler wavelengths (left axis) are plotted as a function of crystal temperature. Also shown in the resulting H-CARS and local EP-CARS signals. The addressed Raman shift as a function of crystal temperature is plotted on the right axis. (a) Second-order chain and (b) third-order chain. F, 2F, and 3F are the fundamental, second harmonic, and third harmonic wavelength of the laser, respectively.

approach is insensitive to self-phase modulation, two-photon absorption, and thermal lensing that could confuse SRS signals. It requires one extra modulator and more complex electronics but it allows for the selective detection of multiple substances even if their resonances overlap [12].

References

1. C. L. Evans and X. S. Xie, "Coherent anti-Stokes Raman scattering microscopy: chemical imaging for biology and medicine," Annu. Rev. Anal. Chem. **1**, 883–909 (2008).
2. Y. Yoo, D. Lee, and H. Cho, "Differential two-signal picosecond-pulse coherent anti-Stokes Raman scattering imaging microscopy by using a dualmode optical parametric oscillator," Opt. Lett. **32**, 3254–3256 (2007).
3. F. Ganikhanov, C. Evans, B. Saar, and X. Xie, "High-sensitivity vibrational imaging with frequency modulation coherent anti-Stokes Raman scattering (FM CARS) microscopy," Opt. Lett. **31**, 1872–1874 (2006).
4. G. Marowsky and G. Lüpke, "CARS-background suppression by phase-controlled nonlinear interferometry," Appl. Phys. B **51**, 49–51 (1990).
5. E. Potma, C. Evans, and X. Xie, "Heterodyne coherent anti-Stokes Raman scattering (CARS) imaging," Opt. Lett. **31**, 241–243 (2006).
6. M. Jurna, J. P. Korterik, C. Otto, and H. L. Offerhaus, "Shot noise limited heterodyne detection of CARS signals," Opt. Express **15**, 15207–15213 (2007).
7. M. Jurna, J. P. Korterik, C. Otto, J. L. Herek, and H. L. Offerhaus, "Background-free CARS imaging by phase sensitive heterodyne CARS," Opt. Express **16**, 15863–15869 (2008).
8. A. Volkmer, L. Book, and X. Xie, "Time-resolved coherent anti-Stokes Raman scattering microscopy: Imaging based on Raman free induction decay," Appl. Phys. Lett. **80**, 1505–1507 (2002).
9. A. Voroshilov, C. Otto, and J. Greve, "Secondary structure of bovine albumin as studied by polarization-sensitive multiplex CARS spectroscopy," Appl. Spectrosc. **50**, 78–85 (1996).
10. J. Cheng, L. Book, and X. Xie, "Polarization coherent anti-Stokes Raman scattering microscopy," Opt. Lett. **26**, 1341–1343 (2001).
11. M. Jurna, J. Korterik, C. Otto, J. Herek, and H. Offerhaus, "Vibrational phase contrast microscopy by use of coherent anti-Stokes Raman scattering," Phys. Rev. Lett. **103**, 043905 (2009).
12. M. Jurna, E. T. Garbacik, J. P. Korterik, C. Otto, J. L. Herek, and H. L. Offerhaus, "Visualizing resonances in the complex plane with vibrational phase contrast coherent anti-Stokes Raman scattering," Anal. Chem. **82**, 7656–7659 (2010).
13. P. Chen, "Rejection of background light using single-wavelength detection in nonlinear Raman spectroscopy," Appl. Spectrosc. **51**, 376–379 (1997).
14. Y. Fu, H. Wang, R. Shi, and J. Cheng, "Characterization of photodamage in coherent anti-Stokes Raman scattering microscopy," Opt. Express **14**, 3942–3951 (2006).
15. M. Balu, T. Baldacchini, J. Carter, T. Krasieva, R. Zadoyan, and B. Tromberg, "Effect of excitation wavelength on penetration depth in nonlinear optical microscopy of turbid media," J. Biomed. Opt. **14**, 010508 (2009).
16. C. W. Freudiger, W. Min, B. G. Saar, S. Lu, G. R. Holtom, C. He, J. C. Tsai, J. X. Kang, and X. S. Xie, "Label-free biomedical imaging with high sensitivity by stimulated Raman scattering microscopy," Science **322**, 1857–1861 (2008).